Supplemental Material:
Nematic spin correlations pervading the phase diagram of $FeSe_{1-x}S_x$

Ruixian Liu,[1] Wenliang Zhang,[2] Yuan Wei,[2] Zhen Tao,[1,2] Teguh C. Asmara,[2]
Yi Li,[1] Vladimir N. Strocov,[2] Rong Yu,[3] Qimiao Si,[4] Thorsten Schmitt,[2,*] and Xingye Lu[1,†]

[1]*Center for Advanced Quantum Studies and Department of Physics, Beijing Normal University, Beijing, 100875 P. R. China*

[2]*Photon Science Division, Swiss Light Source, Paul Scherrer Institut, CH-5232 Villigen PSI, Switzerland*

[3]*Department of Physics, Renmin University of China, Beijing 100872, China*

[4]*Department of Physics and Astronomy, Rice Center for Quantum Materials, Rice University, Houston, TX 77005, USA*

1. Sample growth and characterization

High-quality $FeSe_{1-x}S_x$ single crystals with self-cleaved edges along the tetragonal $[100]_T$ direction were synthesized using the chemical vapor transport technique with KCl-$AlCl_3$ as the flux [1]. The doping levels are determined with Energy Dispersive Spectroscopy (EDS) and confirmed by resistivity measurements. The typical size of the single crystals is ~1*1*0.1 mm^3. Sulfur content x is determined by energy dispersive spectroscopy (EDS) and confirmed by in-plane resistivity measurements (Fig. S1(a)). The short vertical bars in Fig. S1(a) mark the structural transition temperatures (T_S). With increasing x, T_S is suppressed gradually and finally vanishes at $x \approx 0.17$. To determine the nematic quantum critical point (NQCP) accurately, we show in Fig. S1(b) the $T^{1.5}$ dependence of the resistivity curves, which can be well fitted with a linear behavior outside the nematic phase and indicate $x_{QCP} \approx 0.17$ [2]. Therefore, $FeSe_{1-x}S_x$ hosts an electronic nematic state for $x < 0.17$ ($T<T_S$), an NQCP at $x \approx 0.17$, and the tetragonal phase at $x > 0.17$ (and $T>T_S$ for $x \leq 0.17$).

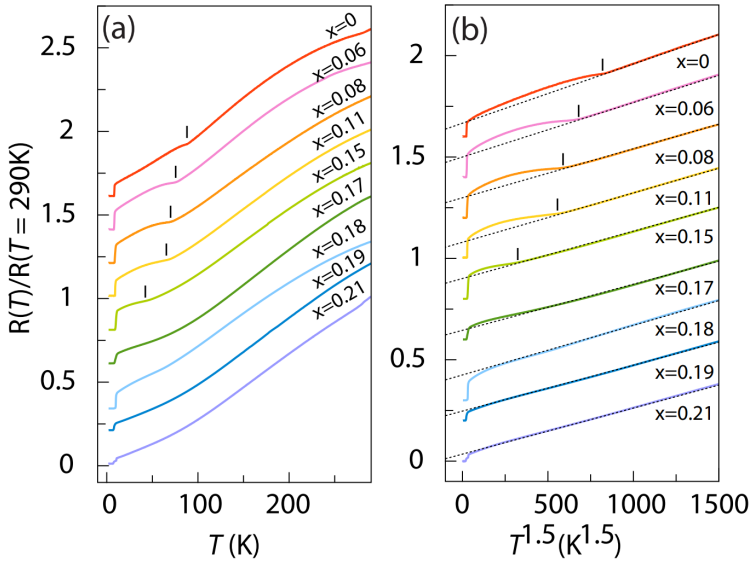

FIG. S1. (a-b) The in-plane resistivity normalized to the data for T=290K, measured by a standard

four-probe method, as a function of T (temperature) (a) and $T^{1.5}$ (b) for the series of dopings of $FeSe_{1-x}S_x$ used in this study. The black vertical bars mark the structural transition temperatures. The resistivity curves are shifted vertically for the reason of clarity.

2. Characterization of the uniaxial strain

In order to investigate the nematic spin correlations in $FeSe_{1-x}S_x$, we employ a uniaxial-strain device (Fig. S2(c)) to study the spin-excitation anisotropy between $S_h(q_{\|})$ and $S_k(q_{\|})$ [3]. The device is designed based on differential thermal expansion coefficients of an aluminum frame ($\alpha \approx -24\times10^{-6}$/K) and internal invar-alloy ($\alpha \approx -2\times10^{-6}$/K) blocks with a titanium (Ti) sample platform [3]. The Ti platform with a neck in the center bridges the two invar-alloy blocks (Fig. S2). The aluminum, invar alloy, and Ti bridge of the strain device are assembled with epoxy Stycast 2850FT. While cooling, the difference in thermal contraction between the outer aluminum frame and the inner invar-alloy blocks and the Ti platform can generate a sizeable uniaxial strain up to $\varepsilon \equiv \varepsilon_{xx}-\varepsilon_{yy} \approx -0.8\%$ on the neck of the Ti bridge. Such a uniaxial strain can be transferred to the $FeSe_{1-x}S_x$ single crystal glued on the Ti bridge via epoxy Stycast 1266 or Stycast 2850FT. The uniaxial strain of the Ti bridge and $FeSe_{1-x}S_x$ single crystal can be accurately characterized by tracking the relative displacements of some specific spots on the platform and the sample using a microscope camera system [4], for which the sample is loaded in a continuous-flow helium cryostat with an optical window (Janis ST500). Note that the strain characterization can only be performed after the RIXS experiment. Thus, this could lead to an underestimation of the uniaxial strain as the warming-cooling cycling could relax the strain a little bit. We found in our tests that the uniaxial strain changed not much (<20%) after several warming-cooling cycles.

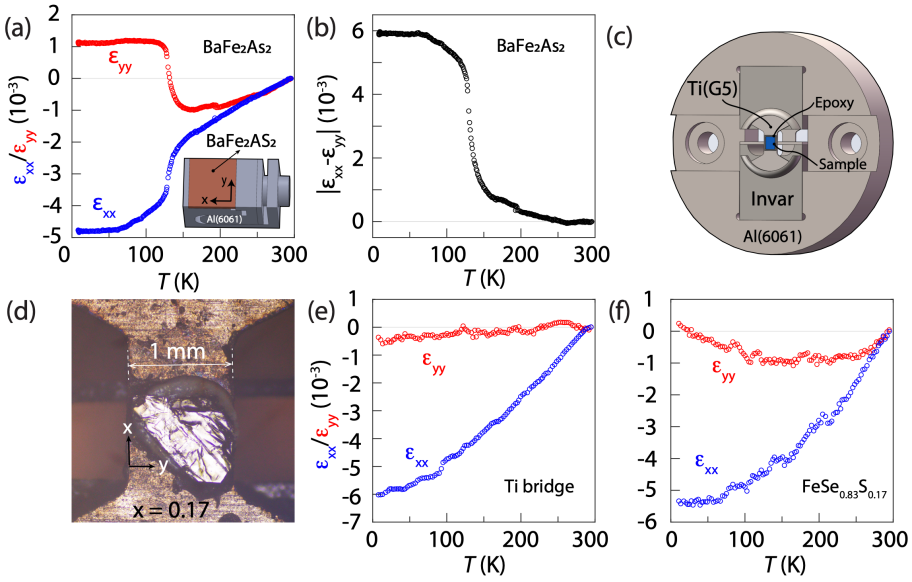

FIG. S2. (a) Anisotropic strain measured on the surface of a uniaxial-pressure detwinned $BaFe_2As_2$ single crystal. The inset shows a mechanical uniaxial-pressure device driven by a screw and a spring washer. (b) The uniaxial strain of $BaFe_2As_2$ defined as $\varepsilon \equiv \varepsilon_{xx}-\varepsilon_{yy}$. As the orthorhombic lattice

distortion is defined as δ=(a-b)/(a+b), we have ε≈-2δ for the orthorhombic state of a detwinned sample. (c) Schematic of the uniaxial-strain device based on differential thermal expansions between the aluminum frame and the inner invar-alloy blocks. (d) Optical micrograph of the $FeSe_{0.83}S_{0.17}$ single crystal glued on a titanium platform, taken after RIXS measurements. (e), (f) The uniaxial strains measured on the Ti bridge (e) and the $FeSe_{0.83}S_{0.17}$ single crystal (f).

We first characterized the uniaxial strain (orthorhombic lattice distortion) on a $BaFe_2As_2$ single crystal detwinned by a uniaxial-pressure detwinning device (the inset of Fig. S2(a)). Installing the device in the helium cryostat ST500, we can take a series of photos with a microscope during cooling. Employing the Digital Image Correlation Engine (DICe) software [4], we can track the relative displacement of features on the surface of the sample while cooling. The measured strains $\varepsilon_{xx}=(b-b_0)/b_0$, $\varepsilon_{yy}=(a-a_0)/a_0$ of detwinned $BaFe_2As_2$ along x (*b* axis) and y (*a* axis) directions are shown in Fig. S2(a). As the orthorhombic lattice distortion is defined as δ=(a-b)/(a+b), we have ε≈ε_{xx}-ε_{yy}≈-2δ. The measured ε in Fig. S2(b) (ε≈ε_{xx}-ε_{yy}≈-0.6%) is indeed consistent with the orthorhombic lattice distortion (δ=0.36% at $T \ll T_S \approx 138$K) of uniaxial-pressured-detwinned $BaFe_2As_2$ measured by high-resolution neutron and x-ray diffraction measurements [5]. This demonstrates that the optical micrograph method is effective in determining the uniaxial strain of samples. Note that the uniaxial strain of $BaFe_2As_2$ at T=300K was set to zero. It should be ~0.05% under a typical uniaxial pressure (~20MPa) [5].

For the RIXS measurements, $FeSe_{1-x}S_x$ samples were cleaved in situ in an ultrahigh vacuum at a based temperature (T = 15 ~ 20 K) [6]. Figure S2(d) shows an optical micrograph of a $FeSe_{0.83}S_{0.17}$ single crystal taken after the RIXS experiment. Using the same method, we measured the uniaxial strain on the surface of the sample and Ti platform. Figure S2(e) and S2(f) show the characterization of the uniaxial strain measured on the Ti platform (Fig. 2(e)) and the $FeSe_{0.83}S_{0.17}$ crystal (Fig. S2(f)) as shown in Fig. S2(d). The calculated uniaxial strain is ε=ε_{xx}-ε_{yy}≈-0.6%.

3. Additional RIXS spectra of strained and unstrained $FeSe_{1-x}S_x$

For the RIXS measurements, all the spectra were collected with π polarization. We define the momentum transfer **q** in reciprocal space as $\mathbf{q} = H\mathbf{a}^* + K\mathbf{b}^* + L\mathbf{c}^*$, where *H*, *K*, *L* are Miller indices and $\mathbf{a}^* = \mathbf{e}_a\, 2\pi/a$, $\mathbf{b}^* = \mathbf{e}_b\, 2\pi/b$, and $\mathbf{c}^* = \mathbf{e}_c\, 2\pi/c$ are reciprocal lattice unit (r.l.u.) vectors with $a \approx 5.3$ Å, $b \approx 5.3$ Å and $c \approx 5.5$ Å. All spectra in this paper are normalized to the integrated intensity of the fluorescence signal in the energy loss range of 1 ~ 10 eV. Figure S3(a) and Figure S3(c) show the momentum-dependent RIXS spectra of unstrained $FeSe_{1-x}S_x$ samples (x = 0.08, 0.18) with momentum transfer along *H* direction at T = 15K. Figure S3(b) shows RIXS spectra of uniaxial-strained $FeSe_{0.89}S_{0.11}$ (x = 0.11) at T = 15K and 100K along *H* and *K* direction, measured at Fe L_3-edge. The spin-excitation anisotropy gradually decreases at a higher temperature. Magnetic excitation spectra along [*H, H*] direction in $FeSe_{0.94}S_{0.06}$ and $FeSe_{0.81}S_{0.19}$ at T = 20K are shown in Figure S3(d-e). Dispersive magnetic excitations

are observed as a broad peak in the low-energy region. With increasing momentum transfer $q_{\parallel}$ the energy position of the magnetic excitations shift away from the elastic peak and the intensity increases.

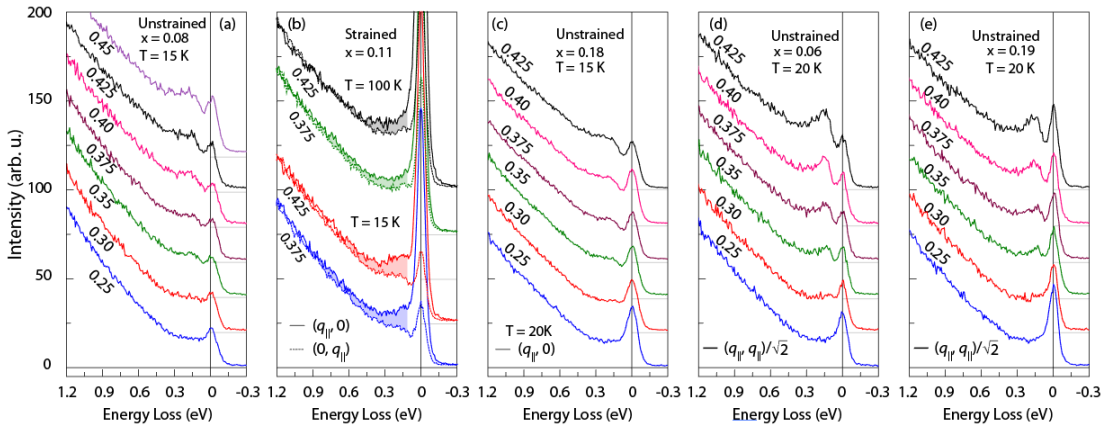

FIG. S3. Momentum-dependent RIXS spectra measured on unstrained (x = 0.08, 0.18, 0.06, and 0.19) and uniaxial-strained (x = 0.11) $FeSe_{1-x}S_x$ samples. (a), (c) $q_{\parallel}$-dependent RIXS spectra along H direction of unstrained x = 0.08 and 0.18 samples at T = 15 K. (b) RIXS spectra along H (solid curves) and K (dashed curves) directions of a uniaxial-strained x = 0.11 sample at T = 15 and 100K. The colored areas mark the difference between $I_h(q_{\parallel})$ and $I_k(q_{\parallel})$. (d), (e) RIXS spectra along [H, H] directions of unstrained x = 0.06 and 0.19 samples at T = 20K.

4. Fitting of the RIXS spectra of uniaxial-strained $FeSe_{0.83}S_{0.17}$

In order to quantitatively analyze all RIXS spectra, we employ an energy resolution-limited Gaussian function, a quadratic polynomial, and a general damped harmonic oscillator function to fit elastic peak scattering (I_{el}), fluorescence background (I_{fluo}(E)), and magnetic excitation ($S(E)$), respectively [6, 7].

The RIXS spectrum is expressed as:

$$I(E) = I_{fluo}(E) + S(E) + I_{el}(E) \qquad (1)$$

The elastic peak (Gaussian functions) is described by:

$$I_{el} = a_0 \exp\left(-\ln(2) * \frac{(x-x_0)^2}{dx^2}\right) \qquad (2)$$

where x_0 is the center of the elastic peak.

The fluorescence response in iron-based superconductors (FeSC) can be captured by (quadratic polynomial functions),

$$I_{fluo} = (bE^2 + aE) \cdot \left(1 - g_\gamma\right) + I_0 \exp(-\alpha E) \cdot \ g_\gamma + G \qquad (3)$$

with

$$g_\gamma = (\exp\left(\frac{E+E^*}{\Gamma}\right) + 1)^{-1} \qquad (4)$$

$$G = A_0 \exp\left(\frac{(E+E_S)^2}{2\sigma^2}\right) \qquad (5)$$

where G is a Gaussian function.

The first and second term of formula (3) describe the low energy loss with second-order polynomial behavior and the high-energy loss with exponential behavior of the fluorescence line, respectively. g_γ generates a smooth connection between these two behaviors.

The damped magnetic excitation in FeSC (damped harmonic oscillator function) is described as:

$$S(q,E) = A\frac{E_0}{1-e^{-\beta E}}\frac{2\gamma E}{\left(E^2-{E_0}^2\right)^2+(E\gamma)^2} \qquad (6)$$

$\beta = \frac{1}{k_B T}$ (k_B is Boltzmann constant).

where E_0 is the underdamped energy and γ describes the excitation lifetime (the damping rate).

Figure S4 (a-f) show the fitting of the RIXS spectra $I_h(q_{\|})$ and $I_k(q_{\|})$ for the uniaxial-strained $FeSe_{0.83}S_{0.17}$. The results reveal strong anisotropy between the spin excitations $S_h(q_{\|})$ and $S_k(q_{\|})$ in the whole $q_{\|}$ range measured. RIXS spectra along [H, H] direction and their fitting are shown in Fig. S4 (g-l). All spectra are collected at T = 20 K and the fitting results are shown and discussed in the main text.

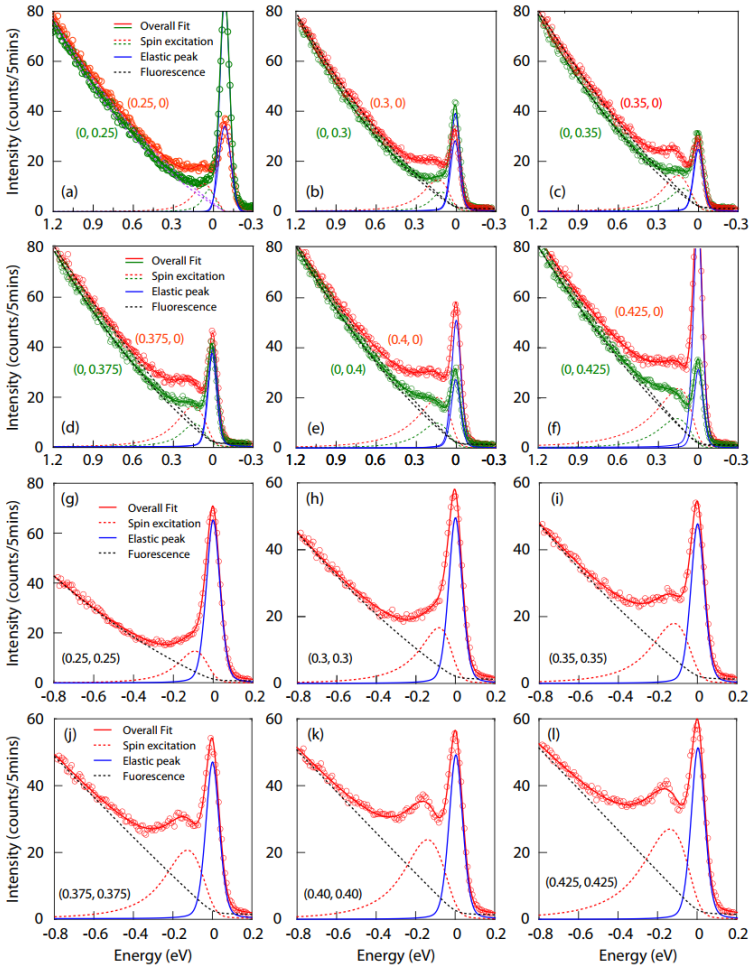

FIG. S4. Fitting of the RIXS spectra for uniaxial-strained x=0.17, measured at T = 20 K. (a-f) RIXS spectra along [H, 0] (red open circles) and [0, K] (green open circles) directions. (g-l) RIXS spectra along [H, H] (red open circles) direction, which is not affected by uniaxial strain. The red and green dashed curves, black dashed curves, and solid blue curves are fitting components of spin excitations, fluorescence contribution, and the elastic peak, respectively. The red and green solid curves represent the overall fitting of the RIXS spectra.

5. Uniaxial stress/strain and nematic susceptibility

In FeSCs, twinning domains with two orthogonal directions usually form in the nematic (orthorhombic) state, which average the electronic properties along the intrinsic a/b axes and hinders the studies of the electronic nematicity [9]. Because a is slightly larger than b, it was found that uniaxial stress/strain along the a/b axes can detwin the FeSC single crystals and therefore help to study the intrinsic electronic properties.

On the other hand, it was found that uniaxial stress used to detwin the sample can also induce a pronounced electronic anisotropy (nematicity) in a temperature range above T_s, indicating the uniaxial strain (ε) is directly coupled to the electronic nematicity (ψ) in the nematic fluctuating regime at T>T_s.

The effect of electron-lattice coupling (ΔE=-$\lambda\psi\varepsilon$, λ is the coupling parameter) can be modeled by a Ginzburg-Landau free energy [10]:

$$F = \frac{a}{2}\psi^2 + \frac{b}{4}\psi^4 + \frac{c}{2}\varepsilon^2 + \frac{d}{4}\varepsilon^4 - \lambda\psi\varepsilon - h\varepsilon$$

In ref. [10], the authors find $d\psi/d\varepsilon=\lambda/a=\lambda/[a_0(T-T^*)]$ that can describe the resistivity change ($\eta=\Delta\rho/\rho_0$) under elastic strain very well ($d\psi/d\varepsilon \sim d\eta/d\varepsilon$) at $T>T_s$. This work demonstrated that the nematicity is driven by certain electronic degree of freedom (rather than a structural origin) and established the elastoresistance as a measure of the *static* nematic susceptibility $\chi_{nem}= d\psi/d\varepsilon$, in which the uniaxial strain is an external perturbating field to induce a detectable change in electronic properties. In previous works, it was found that the electronic anisotropy is linearly coupled to the uniaxial strain at $|\varepsilon|<\sim$0.2-0.3. At higher strain (still in the elastic strain range), the electronic anisotropy might saturate [11].

For $FeSe_{1-x}S_x$, ref. [8] reported *static* electronic nematic susceptibility derived from elastoresistance measurements [$dR_{xx}/d\varepsilon$, or $(\Delta R/R)_{xx}$ under a fixed ε, with $\varepsilon\sim$0.01%] and showed that the nematic susceptibility exhibits a diverging tendency near the nematic quantum critical point. Although the transport measurements could couple to all channels (charge, spin, and orbital), the *static* transport measurements cannot distinguish which degree of freedom drives the electronic nematicity.

The Fe-L_3 edge RIXS measurements presented in this study, zoom in on the spin (fluctuation) channel directly. More importantly, the elastoresistivity can characterize only static nematic susceptibility $\chi_{nem}(T)$ with q=0 and E=0, while the nematic spin fluctuation $\chi''_{nem}(\mathbf{q}, E, T)$ could be a manifestation of nematic fluctuations with finite momentum and energy.

6. Spin-excitation anisotropy and Nematic spin correlations

The nematic spin correlations refer to the intensity difference of the spin excitations between $\mathbf{Q}_1+\mathbf{q}_x$ and $\mathbf{Q}_2+\mathbf{q}_y$ (denoted by $S_1(q_x+\mathbf{Q}_1, E)$-$S_2(q_y+\mathbf{Q}_2, E)$) (ref. [2] in the main text), in which $\mathbf{Q}_1$=(1, 0), $\mathbf{Q}_2$=(0, 1), and $\mathbf{q}_x$ and $\mathbf{q}_y$ are equivalent reduced wave vectors in the antiferromagnetic (AF) Brillouin zones at $\mathbf{Q}_1$ and $\mathbf{Q}_2$, respectively. Nematic spin correlations are defined in the nematic state (orthorhombic *paramagnetic* state) and the nematic fluctuating regime and are a manifestation of the electronic nematicity in the spin-spin correlation function. Such nematic spin correlations can be directly measured with inelastic neutron scattering. Figure S5(a) shows constant-energy (E = [44, 52] meV) spin excitations measured in a detwinned FeSC sample. The spin-excitation difference between $\mathbf{Q}_1$ and $\mathbf{Q}_2$ is the nematic spin correlations (if we assume it is measured in a pure nematic state without AF order). The one-dimensional cuts in Fig. S5(b) across the signal show the difference clearly.

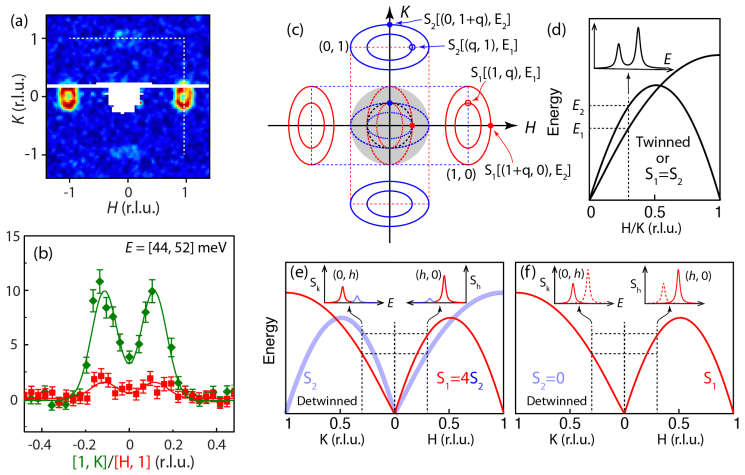

FIG. S5. (a), (b) Constant-energy spin excitations with E=[44, 52]meV measured in detwinned $BaFe_2As_2$. The white dashed lines in (a) mark the trajectories of the one-dimensional cuts in (b). (c) Reciprocal space and Brillouin zone for typical FeSC systems. The red (blue) dashed rectangle are first BZ centering at Γ point associated with $\mathbf{Q}_1 = (1, 0)$ ($\mathbf{Q}_2 = (0, 1)$). The inner (outer) ellipses mark the constant-energy excitations with an energy transfer of E_1 (E_2). (d)-(f) Schematic dispersion for (d) a twinned sample or a sample with no nematic spin correlations ($S_1 = S_2$), (e) a detwinned sample with nematic spin correlations $S_1 > S_2$, and (f) a detwinned sample with S_1 only. The insets in (d)-(f) show the corresponding spectra S_h and S_k.

It is well known that inelastic neutron scattering (INS) measurements of spin excitations require large volume of single crystals. Furthermore, the nematic spin correlations can only be studied in detwinned or uniaxially-strained samples. Such INS experiments are impossible for $FeSe_{1-x}S_x$ as it is extremely challenging to detwin or apply uniaxial strain to a large amount of $FeSe_{1-x}S_x$ single crystals simultaneously, in particular, $FeSe_{1-x}S_x$ single crystals are usually tiny and soft. Thus, we developed the strategy to probe the nematic spin correlations using RIXS (ref. [23] in the main text). RIXS can measure high-energy spin excitations on a small sample. However, the Fe-L_3 RIXS (E_i≈707eV) can cover a limited momentum range in the first BZ (filled gray circle in Fig. S5(c)) and cannot reach $\mathbf{Q}_1$ and $\mathbf{Q}_2$ to reveal the nematic spin correlations directly.

Figure S5 shows how we can connect the spin-excitation anisotropy measured with RIXS to the intrinsic nematic spin correlations. We define the spin-excitation anisotropy as $\phi(q_{\parallel})=S_h(q_{\parallel})/ S_k(q_{\parallel})$, in which $S_h(q_{\parallel})$ and $S_k(q_{\parallel})$ are energy integrated spin excitations measured at $(q_{\parallel}, 0)$ and $(0, q_{\parallel})$, respectively.

In our previous neutron scattering study, we defined the nematic spin correlations as $\psi(E)=[S_1(E)-S_2(E)]/[S_1(E)+S_2(E)]$ (or $\psi(E)=[S_1(\mathbf{q},E)-S_2(\mathbf{q},E)]/[S_1(\mathbf{q},E)+S_2(\mathbf{q},E)]$), where $S_{1,2}(E) = \int S_{1,2}(\mathbf{q}, E)d\mathbf{q}$, and the integral $\int d\mathbf{q}$ runs over the whole BZ. Note $\mathbf{q}$ is a reduced momentum within a BZ.

As shown in Fig. S5(c), the RIXS spectra $S_h(q)$ and $S_k(q)$ measured at $(q, 0)$ (red dot) and $(0, q)$ (blue dot) in the first BZ, can be written as:

$S_h(q)=S_1[(q, 0), E_2] + S_2[(q, 0), E_1]$

$S_k(q)=S_1[(0, q), E_1] + S_2[(0, q), E_2]$

As $S_h(q)>S_k(q)$ at all the momenta measured, the lower limit for $\phi(q)$ is 1, which can be realized in a twinned sample, or a system without nematic spin correlations, as shown in Fig. S5(d). The upper limit for $\phi(q)$ is $\phi_{max}(q)=S_1[(q, 0), E_2]/S_1[(0, q), E_1]$, which can be achieved in a system where S_2 vanishes [Fig. S5(f)]. In $FeSe_{1-x}S_x$, the dispersion and intensity of the spin excitations are almost doping-independent in x=0-0.21, leading to a doping-independent $\phi_{max}(q)$. For a system with nematic state, the spin-excitation anisotropy $\phi(q)$ can reflect the amplitude and energy scale of the nematic spin correlations [Fig. S5(e)].

We have attributed the spin-excitation anisotropy to the electronic nematicity. But it is still meaningful to discuss whether it could be a result of uniaxial strain (i.e., change in the bond lengths). One would expect that the change in bond length will alter the hopping between Fe ions and vary the AF exchange coupling, which might induce a pronounced change in spin excitation, especially the dispersion. In a detwinned $BaFe_2As_2$ sample, the structural transition at T_s≈138K generates an orthorhombic lattice distortion corresponding to $|\varepsilon_{xx}-\varepsilon_{yy}|$~0.72%. However, the energy dispersion does not change across T_s. In our results, the uniaxial strain $|\varepsilon_{xx}-\varepsilon_{yy}|$ ~0.8% applied onto the $FeSe_{0.89}S_{0.11}$ sample far exceeds the detwinning limit, while the extra strain does not induce a detectable change in energy dispersion. In the uniaxially-strained x=0.17 sample, $\varepsilon_{xx}-\varepsilon_{yy}$ ~-0.6% induce a significant change in energy dispersion. However, such large difference in energy dispersion between $S_h(q_\parallel)$ and $S_k(q_\parallel)$ cannot be described by considering such a small change in bond length. Thus, the spin excitation anisotropy cannot be attributed to pure uniaxial strain (the change in bond length).

7. Doping dependence of the spin-excitation anisotropy

Fig. S6(a) (Fig. 4(c) in the main text) plots the doping dependence of the spin excitation anisotropy $\phi(q_\parallel)=S_h(q_\parallel)/S_k(q_\parallel)$. Note that the uniaxial strain applied on these samples are not exactly the same and have some variations. Though the variation of the applied uniaxial strain is large, it is not reasonable to "normalize" the curves to the applied strain as the uniaxial strain could not be linearly coupled to the spin excitation anisotropy at $|\varepsilon| > 0.2\%$ [11].

Here we explain why the variation of the strain does not alter the conclusion that the spin excitation-anisotropy is enhanced near the NQC regime. The largest strain ε ≈-0.8% applied on the x=0.11 sample generates a small (almost the least) $\phi(\varepsilon)$, indicating the effects of uniaxial strain on nematicity is saturated at $|\varepsilon| < 0.8\%$. This is consistent with several prior studies showing that the linear coupling between uniaxial strain and electronic nematicity is only valid in a small range of uniaxial strain. In the orthorhombic state, the effects of uniaxial strain could saturate when the strain exceeds the detwinning threshold (above which the sample is fully detwinned) [11]. Measured with ε≈-0.6% for x=0.15 and 0.17 and ε≈-0.4% for x=0.18, $\phi(\varepsilon)$ in these samples are obviously larger than that in x=0.11,

showing the spin excitation anisotropy is enhanced in the NQCP regime. Compared with the ϕ(ε=-0.4%) in x=0.18, the ϕ(ε) in x=0.21 sample measured with the same ε=-0.4% is apparently smaller, corroborating the enhancement of the spin-excitation anisotropy in the NQC regime. Thus, the conclusion concerning the enhancement of the spin-excitation anisotropy at the NQC regime is valid even though the strain varies a little bit for different dopings.

In a sample without spin excitation anisotropy, we have $S_h(q_\parallel)/S_k(q_\parallel)$=1. Thus, the spin excitation anisotropy induced by uniaxial strain is $[S_h(q_\parallel)/S_k(q_\parallel)$-1]. Assuming the uniaxial-strain induced $[S_h(q_\parallel)/S_k(q_\parallel)$-1] is linearly coupled to the strain ε, the conclusion is still valid, as can be seen from the strain-normalized plot in Fig. S6(b).

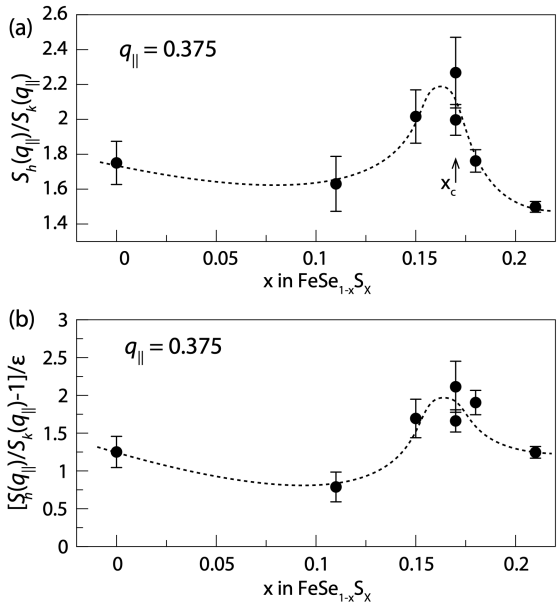

FIG. S6. (a) Doping dependence of the $S_h(q_\parallel)/S_k(q_\parallel)$ with $q_\parallel$ = 0.375. The uniaxial strain applied on the samples are ε≈-0.6% (x=0), ε≈-0.8% (x=0.08), ε≈-0.6% (x=0.15), ε≈-0.6% (x=0.17), ε≈-0.4% (x=0.18), and ε≈-0.4% (x=0.21). (b) Doping dependence of the spin excitation anisotropy $[S_h(q_\parallel)/S_k(q_\parallel)$-1] normalized to ε≈-1%.

Reference:

[1] D. Chareev *et al*., Single crystal growth and characterization of tetragonal $FeSe_{1-x}$ superconductors. Cryst Eng Comm, **15**, 1989-1993 (2013).

[2] M. Bristow *et al*. Anomalous high-magnetic field electronic state of the nematic superconductors $FeSe_{1-x}S_x$. Phys. Rev. Research. **2**, 013309 (2020).

[3] V. Sunko et al., Direct observation of a uniaxial stress-driven Lifshitz transition in Sr_2RuO_4. npj Quantum Materials **4**, 46 (2019).

[4] B. Pan *et al*. Two-dimensional digital image correlation for in-plane displacement and strain

measurement: a review. Meas. Sci. Technol. **20**, 0620001 (2009).
[5] X. Lu *et al.*, Impact of uniaxial pressure on structural and magnetic phase transitions in electron-doped iron pnictides. Phys. Rev. B **93**, 134519 (2016).
[6] X. Lu *et al*. Spin-excitation anisotropy in the nematic state of detwinned FeSe. Nat. Phys. **18**, 806-812 (2022).
[7] J. Pelliciari *et al*., Reciprocity between local moments and collective magnetic excitations in the phase diagram of $BaFe_2(As_{1-x}P_x)_2$. Commun Phys. **2**, 139 (2019).
[8] S. Hosoi *et al.*, Nematic quantum critical point without magnetism in $FeSe_{1-x}S_x$ superconductors. Proc. Natl Acad. Sci. USA **113**, 8139-8143 (2016).
[9] J.-H. Chu *et al.* In-plane resistivity anisotropy in an underdoped iron arsenide superconductor. Science **329**, 824-826 (2010).
[10] J.-H. Chu, H.-H. Kuo, J. G. Analytis, & I. R. Fisher. Diver- gent Nematic Susceptibility in an Iron Arsenide Superconductor. Science **337**, 710-712 (2012).
[11] C. A. Occhialini, J. J. Sanchez, Q. Song, G. Fabbris, Y. Choi, J.-W. Kim, P. J. Ryan, and R. Comin. Spontaneous orbital polarization in the nematic phase of FeSe. Nat. Mater. **22**, 985-991 (2023).